IEICE TRANS. ELECTRON., VOL.E104–C, NO.10 OCTOBER 2021

INVITED PAPER *Special Section on Microwave and Millimeter-Wave Technologies*

Recent Progress in Envelope Tracking Power Amplifiers for Mobile Handset Systems

Kenji MUKAI[†a)], **Hiroshi OKABE**[†], ***Members***, ***and*** **Satoshi TANAKA**[†], ***Senior Member***

SUMMARY The Fifth-Generation new radio (5G NR) services that started in 2020 in Japan use a higher peak-to-average power ratio (PAPR) of a modulated signal with a maximum bandwidth of up to 100MHz and support multi-input/multi-output (MIMO) systems even in mobile handsets, compared to the Third-Generation (3G) and/or Fourth-Generation (4G) handsets. The 5G NR requires wideband operation for power amplifiers (PAs) used in handsets under a high PAPR signal condition. The 5G NR also requires a number of operating bands for the handsets. These requirements often cause significand degradation of the PA efficiency, consequently. The degradation is due to wideband and/or high PAPR operation as well as additional front-end loss between a PA and an antenna. Thus, the use of an efficiency enhancement technique is indispensable to 5G NR handset PAs. An envelope tracking (ET) is one of the most effective ways to improve the PA efficiency in the handsets. This paper gives recent progress in ET power amplifiers (ETPAs) followed by a brief introduction of ET techniques. The introduction describes a basic operation for an ET modulator that is a key component in the ET techniques and then gives a description of some kinds of ET modulators. In addition, as an example of a 5G NR ETPA, the latest experimental results for a 5G ETPA prototype are demonstrated while comparing overall efficiency of the ET modulator and PA in the ET mode with that in the average power tracking (APT) mode.

key words: *5G NR, mobile handset, power amplifier, envelope tracking*

1. Introduction

With strong and rapid demand for large data and high-speed transmissions, mobile communication systems have made remarkable progress in supporting various kinds of multiplexing methods—Code-Division Multiple-Access (CDMA), Long Term Evolution (LTE), and Orthogonal Frequency Division Multiplexing (OFDM)—and the increase in their modulation bandwidth as well as supporting the number of operating bands. The 5G NR, whose service just started in 2020 in Japan, features higher data rates, multiple simultaneous connections, and lower latency, compared to the existing 3G and 4G systems. Mobile handset systems in 5G need to support a modulation bandwidth of up to 100MHz in a category called "FR1 (Frequency Range 1: below 7.125 GHz)", accordingly [1].

For 5G handsets, there is another demand of RF transmitter miniaturization, because an RF transmitter has been becoming more complicated since 4G [2]. Typical RF transmitters for 3G/4G/5G handsets are illustrated in Fig. 1.

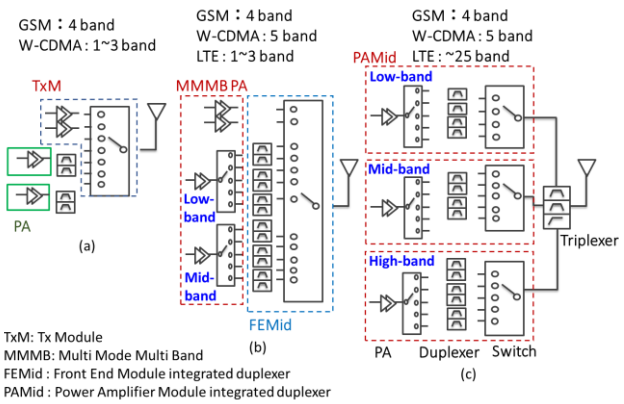

Fig. 1 Block diagrams for Tx architecture for mobile communication systems. (a) 3G systems, (b) early 4G systems, (c) 4G systems.

As illustrated in the figure, we can see that RF front-end loss, which is defined as the transfer loss between a PA and an antenna, has steadily increased with the change in generations.

For example, in 3G handsets, a PA operates only in a single frequency band, and its front-end loss is typically as low as 1 dB [3]–[6]. In contrast, in 4G handsets, some band select switches are placed right after a PA while several frequency bands are covered with one PA. As depicted in the red dotted box of Fig. 1 (b), since the PA module integrates two or three PAs and some band-select switches onto the same laminate, the module was called "MMMB (multi-mode, multi-band)" PA module [7], [8]. The reason why it is called "MMMB" is that the MMMB PA can operate with different kinds of operating modes and operate in different kinds of frequency bands, such as a GSM (Global System for Mobile communication)/EDGE (Enhanced Data Rates for GSM Evolution), 3G, and 4G. In the 4G handsets, a typical RF front-end loss is higher than that of the 3G loss.

In 5G handsets, a triplexer is placed in front of the antenna in order to transmit three different kinds of band (low-, mid-, and high-bands) signals simultaneously, thus allowing inter-band carrier aggregation (CA) even in a handset. However, because the triplexer creates additional transfer loss, a typical RF front-end loss in the 5G handsets is as high as at least 3 dB. As shown in Fig. 1 (c), a PA, a band-select switch, several duplexers, and an antenna switch are integrated on the single laminate operating in each band of low-, mid-, high-bands. This type PA module is often called "PA Module integrated duplexers (PAMid)" [9].

Manuscript received January 13, 2021.
Manuscript revised February 22, 2021.
Manuscript publicized March 19, 2021.

[†]The authors are with Murata Manufacturing Co., Ltd., Nagaokakyo-shi, 617–8555 Japan.
a) E-mail: kenji.mukai@murata.com

DOI: 10.1587/transele.2021MMI0005

As is well known, there are mainly three constraints for 5G handset RF front-ends unlike those for use in base stations: i) limited circuit area, ii) very wideband operation, and iii) limited supply voltage due to Li-ion batteries of a 3.7-V standard voltage. Regarding i) and ii), only three PAs covers a number of operating bands, for example, at least 20 bands. This requires very wideband operation for the PAs: e.g. the low-band ranges from 700 MHz to 915 MHz, the mid-band ranges from 1.7 GHz to 2.01 GHz, and the high-band ranges from 2.3 GHz to 2.7 GHz. These ranges mean a relatively wide fractional bandwidth from 8.5% to 27%. In addition, as shown in Fig. 1, since one duplexer necessary for each supporting band and one low-pass filter necessary for each TDD band are necessary for 4G/5G operation, the filter block occupies most of area in the RF front-end. The circuit area given for the PAs is strictly restricted, consequently. From viewpoints of the limited area and wide operating bandwidth, it is not easy to use Doherty amplifier configuration for the PAs even in the case of high PAPR signals such as 5G OFDM signals.

In handset PAs, the reduction in current dissipation under a relatively low output power operation as well as under a high output power operation is strongly required for extending battery life in practical use [10].

To address this requirement, a supply collector/drain voltage control technique, so called "Average Power tracking (APT)," has been mainly employed for 3G and early 4G handset PAs. In APT, with a buck or buck/boost DC-DC converter, supply voltage for the PA is gradually or statically varied depending on average output power levels. The typical transition time of the supply voltage is as slow as several msec. or a few sec.

Figure 2 shows a typical example of PA efficiency (power-added efficiency, PAE) versus output power for the conventional single-chain handset PA. In Fig. 2 (a), an example of complementary cumulative distribution function (CCDF) vs. PAPR is plotted for various kinds of modulation signals used for 3G/4G/5G. Figure 2 (b) shows PAE vs. output power characteristics under APT control as a parameter of the various modulation signals. In Fig. 2 (b), output power is varied depending on supply voltage and PAE against each output power level that satisfies ACLR < -35 dBc is plotted. Figures 2 (c) and 2 (d) show examples for PAE and ACLR under the APT mode operation. In the APT mode, collector/drain voltage for the handset PA is controlled while the PA satisfies ACLR specifications (less than -33 dBc) specified by 3GPP. As can be seen in Figs. 2 (a) and (b), the difference in PAPR between 3G and 5G is as large as approximately 5 dB, thereby resulting in the significant PAE degradation of 15 to 20 percentage points under the 5G operation. Thus, because high PAPR signals such as 5G cause unacceptable PAE degradation, another efficiency enhancement technique instead of APT is indispensable to the handset PAs. Envelope tracking (ET) technique is one of the most effective ways to improve the efficiency under the above constraints.

This paper gives recent progress in ET power amplifiers (ETPAs) followed by a brief introduction of ET techniques. Section 2 gives an introduction of a basic operation for an ET modulator that is a key component in the ET techniques then describes some kinds of ET modulators. Section 3 describes recent progress in the ET techniques. In Sect. 4, as an example of a 5G NR ETPA, the latest experimental results for a 5G ETPA prototype are demonstrated while comparing overall efficiency between ET and APT modes. Finally, Sect. 5 concludes this paper.

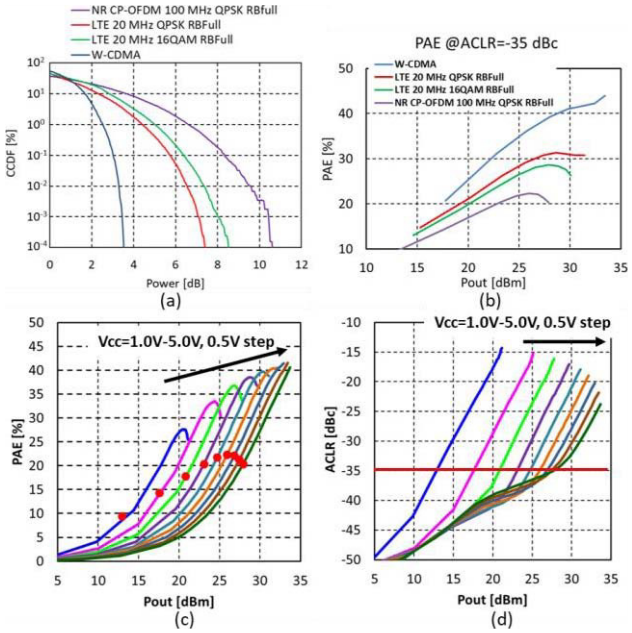

Fig. 2 (a) CCDF for each modulated signal, (b) PAE versus Pout under the APT operation for various signal modulations, (c) PAE versus Pout in the APT mode under 5GNR CP-OFDM 100MHz QPSK modulated signal condition, and (d) ACLR versus Pout in the APT mode under the same 5GNR condition.

2. Envelope Tracking Power Amplifier (ETPA)

ET technique close to their present styles were proposed by A.A.M. Saleh and D.C. Cox [11] and B.D. Geller, F.T. Assal, R.K. Gupta, and P.K. Cline [12].

Much attention to the ET techniques was not drawn from the very beginning of the advent of cellular communications. The reason is that Global System for Mobile (GSM) systems and Advanced Mobile Phone System (AMPS) adopted for the second generation (2G) handsets employed constant envelope signals, allowing PAs to operate with a high efficiency of over 50%.

In contrast, the 3G (CDMA) and 4G (LTE) handsets mainly handle linear modulation signals based on multi-level modulation signals such as QPSK, 16QAM, and 64QAM for improving spectrum efficiency. As a result, high PAPR modulation signals have become very popular, thereby causing unacceptable degradation of the PA efficiency by approximately 10 percentage points or larger.

As mentioned in Introduction, in the 5G handsets, the PAs have to support more multi-level modulation signals

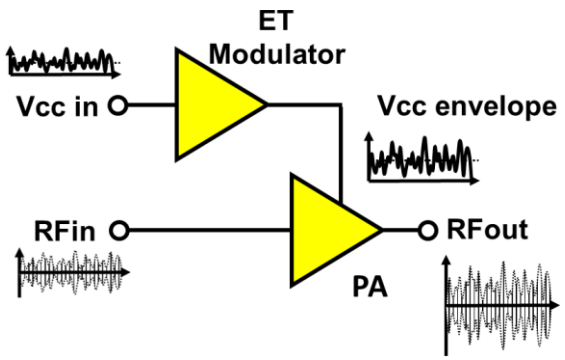

Fig. 3 Simplified block diagram for ETPA.

such as 256QAM as well as a wideband operation of up to 100 MHz, thus involving further efficiency degradation.

In addition, as explained in Fig. 1, the increased front-end loss in the 5G handsets poses the increase in peak output power for the PAs.

As mentioned previously, in the 3G and the early 4G handsets that do not use relatively high PAPR signals, current reduction under low output power operation was strongly required for the handset PAs. Therefore, APT control, so-called V_{cc} control, is incorporated into the handsets. However, the APT control is not effective for high PAPR modulated signals such as 64QAM and 256QAM.

Thus, as one of the most effective candidates to improve efficiency under a high PAPR signal condition, ET techniques have attracted attention from handset manufacturers and PA designers [13], [14]. In particular, the ET techniques have attracted increasing attention from them since the demonstration of fully integrated CMOS ET modulators [15]. The reason why the ET techniques are suitable for handset PAs is that the techniques can easily enhance the efficiency of the conventional PAs, not circuit-area-consuming Doherty PAs. In addition, the ET techniques enable high efficiency operation without a not-negligible efficiency drop between a nominal backed-off power level and a saturation power level, unlike the usual Doherty PAs. In contrast, in the usual two-way Doherty PA's, a not-negligible efficiency drop is often observed, particularly in the case of the target backed-off level of more than 6 dB, resulting in the reduction in overall efficiency.

Currently, a number of commercially available Si-based integrated ET modulators are available to handset PA designers.

2.1 Fundamentals of Envelope Tracking Technique

The ET techniques are implemented by varying collector/drain supply voltage of the PAs so that the voltage can follow an envelope of a modulated signal. This means that the PA can be always operated in a near saturated power region, consequently allowing the PA to operate with high efficiency even in a relatively low output power region such as a nominal backed-off power level.

Figure 3 shows a simplified block diagram of a typical

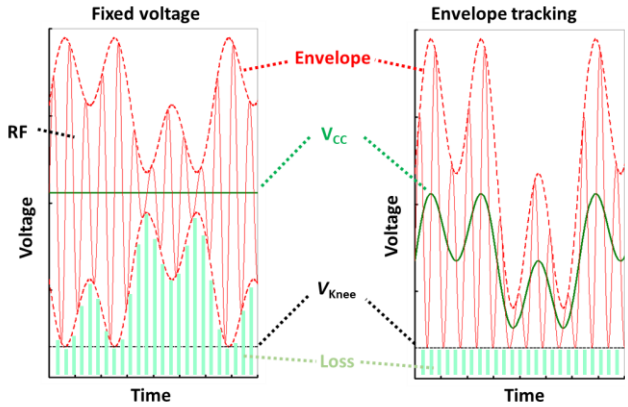

Fig. 4 Time domain supply voltage waveform examples in fixed supply voltage mode and ET mode.

ETPA. The ETPA consists of an ET modulator and a PA, where the collector voltage (V_{cc}) is supplied as an envelope output from the ET modulator. The input signal of the ET modulator is generated by a D/A converter on the RFIC.

The time domain supply voltage waveforms for the fixed supply voltage (V_{cc}) mode and the ET mode are compared in Fig. 4. In the ET mode, as the envelope signal becomes a low level, V_{cc} becomes low, whereas in the fixed mode, the constant V_{cc} is supplied even in low envelope signal levels. As a result, we can see that ET operation can suppress the waste power dissipation of the PA in the low envelope signal levels. In high envelope signal levels, the ET modulator increases V_{cc}, compared to the fixed V_{cc} mode. This means that the ETPA can deliver higher output power than the fixed mode PA can. This power enhancement helps deliver the required peak output power without changing transistor size of the PA. In other words, the enhancement helps compensate for the increased front-end loss in 5G handsets.

The overall efficiency of the ETPA can be given by the following equation:

$$\eta_{\mathrm{ETPA}} = \eta_{\mathrm{mod}} \times \eta_{\mathrm{PA}} \tag{1}$$

where η_{ETPA} is the overall efficiency of the ETPA, η_{mod} is the efficiency of ET modulator, and η_{PA} is the efficiency of the PA. In Eq. (1), since in the ET mode, the PA can always operate in a near saturated power region regardless of envelope signal levels, we can presume that the efficiency of the PA is quite high. On the basis of this presumption, we can expect that the ETPA will always operate with high efficiency as long as the efficiency of the ET modulator is kept very high over the dynamic range of the envelope signal.

Regarding the ETPA operation, there are two technical issues. The first is a simultaneous pursuit of an operational bandwidth and efficiency in the ET modulator. The second is to maintain linearity and high efficiency in the PA. The pursuit of the bandwidth and efficiency in the ET modulator will be described in detail in Sect. 2.3.

In ETPAs, since the PAs operate in a near saturation region, AM-AM and AM-PM characteristics are not so flat,

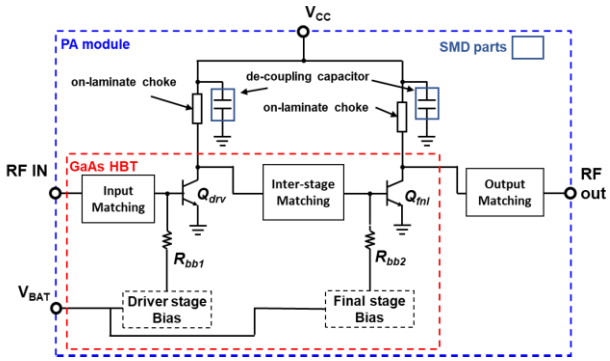

Fig. 5 Simplified schematic for Class-AB biased two-stage PA [20].

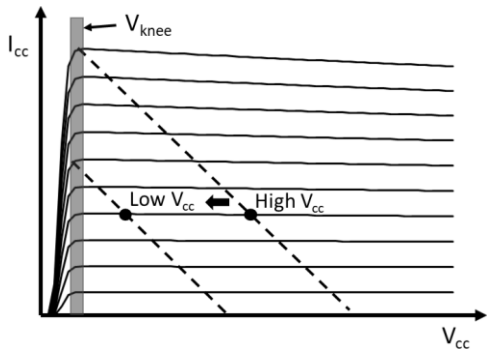

Fig. 6 Loadline examples for Class-AB biased GaAs HBT power stage.

especially in the near saturated power region. Therefore, current ETPAs utilized in practical handsets are supported by a digital predistortion (DPD) technique in order to make the AM-AM/AM-PM characteristics as flat as possible [16]–[19]. This DPD is integrated into an RFIC.

In regard to the DPD, however, the DPD that does not account for the memory effect of the PAs is usually employed in handsets from viewpoints of cost, circuit-size, and current dissipation. Such a DPD is often called "memory-less DPD." Here, the memory effect will be explained in Sect. 4.1. The use of the memory-less DPD implies that it is essential to operate the PA under an optimum condition with regard to the linearity and efficiency, compared to the memory DPD incorporated into the usual base stations. In the next subsection, we describe how to maintain the linearity and high efficiency operation in the PAs.

2.2 Envelope Shaping Function for ETPA

A simplified schematic for a typical handset PA is shown in Fig. 5. The PA is based on a Class-AB biased two-stage HBT configuration, and is still used in current handsets. Except for the output matching and bypass capacitors, most of the PA is integrated on an HBT MMIC die.

As mentioned previously, in the ET operation, V_{cc} varies with envelope signals. Figure 6 illustrates two loadline examples on an I_{ce}-V_{ce} curves in a HBT power stage. These two loadlines correspond to low V_{cc} and high V_{cc}

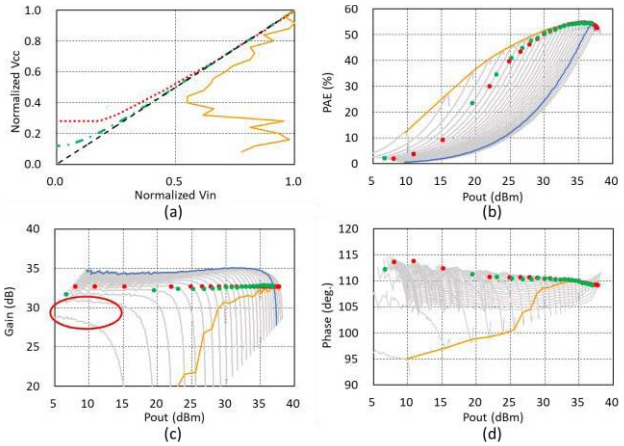

Fig. 7 Examples for (a) envelop shaping function and (b)-(d) waterfall characteristics of PAE, gain and transfer phase shift, where (red dot) iso-gain, (green dot) de-troughing, and (orange line) peak efficiency are also plotted.

states in the ET operation. In the low V_{cc} state, voltage and current swing becomes small, and output power becomes low, accordingly. On the contrary, in the high V_{cc} state, high output power is delivered, because both the swings become large.

Figure 7 (a) shows examples of typical V_{in}-V_{cc} relationship in the ET modulator, where V_{in} denotes the envelope input signal amplitude. Figures 7 (b), (c), and (d) show measured examples for PAE, gain, and transfer phase shift versus output power (P_{out}) characteristics in an HBT PA shown in Fig. 5, In the figures, the parameter is V_{cc}, and V_{cc} is swept from 0.2 V to 5.6 V with a 0.2-V step. Please note that gain vs. P_{out} is called "AM-AM characteristics," and transfer phase shift vs. P_{out} is called "AM-PM characteristics." Figures 7 (b), (c) and (d) are often called "waterfall characteristics." As shown in Figs. 7 (c) and (d), we usually observe gain degradation and a large phase shift as V_{cc} approaches to the knee voltage (V_{knee}) depicted in Fig. 6. The reason is that the reduced V_{cc} increases a feedback capacitance (base-to-collector capacitance) of the HBT power stage.

In the ET operation, on the basis of the above waterfall characteristics, we need to determine the optimum relationship between V_{in} and V_{cc}. This relationship is "envelope shaping function," [21]–[24] and Fig. 7 (a) shows its examples. A typical V_{cc} range is from 1.0V up to 5.0 V. Since input power is proportional to a square of V_{in} and P_{out} is also proportional to a square of V_{cc}, the envelope output voltage (V_{cc}) is basically determined so that V_{cc} can be proportional to a square root of V_{in}.

In addition, from a viewpoint of the linearity and efficiency, we need to determine the envelope shaping function so that the PA can keep AM-AM/AM-PM characteristics as flat as possible while maintaining high efficiency. A "Iso-gain" curve is well known as the most popular envelope shaping function. As shown in Fig. 7, the "iso-gain" curve traces constant gain plots, keeping quite flat AM-AM/AM-PM characteristics [25], [26]. Although the traced

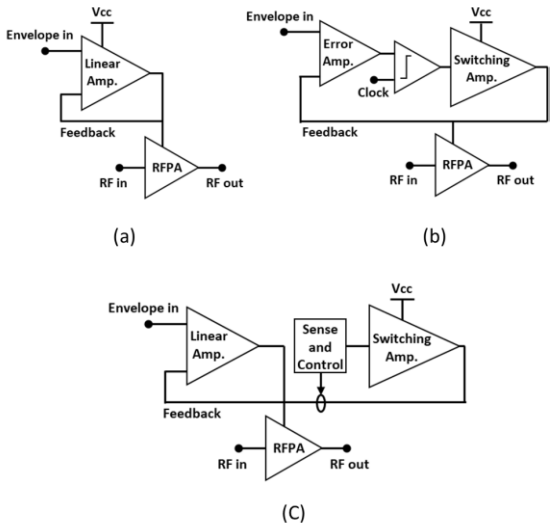

Fig. 8 ET modulator configurations: (a) linear regulator type, (b) switching regulator type, and (c) hybrid type.

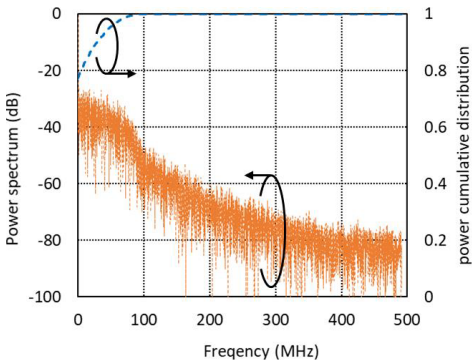

Fig. 9 Envelope characteristics (power spectrum and power cumulative distribution) under CP-OFDM QPSK 100 MHz full resource block modulated signal.

efficiencies for the "iso-gain" curve are a bit lower than the peak efficiencies (orange line in Fig. 7), we can see that the variation of gain and phase is well suppressed, compared to the case where the peak efficiencies are traced.

In Fig. 7 (c), a large gain drop at low V_{cc} near V_{knee} is observed, as indicated with red circle. This drop prevents an ideal "iso-gain"-based control, consequently causing unacceptable degradation of AM-AM/AM-PM curves. To avoid this degradation, we often apply "de-troughing" to the envelope shaping function [27], as depicted in the green line in Fig. 7 (a). This "de-troughing" is applied at a low V_{cc} (e.g. 0.6 V) close to V_{knee} (e.g. 0.4 V). The de-troughing usually reduces the bandwidth of the envelope signal waveform and the sensitivity to time misalignment of the ET system [28]. The transition between the linear region and the de-troughed value is adjusted to maximize efficiency and minimize nonlinearity and memory effects (green dot in Fig. 7). The envelope shaping function including "de-troughing" used in Fig. 7 is given by

$$V_{env}(t) = V_{ccmax} \cdot \left[|x_{in}(t)| + b \cdot e^{-\frac{|x_{in}(t)|}{b}} \right], \quad (2)$$

where V_{ccmax} is the peak envelope voltage, $|x_{in}(t)|$ is the normalized input RF signal amplitude, and b is the "de-troughing" ratio given by $\frac{V_{ccmin}}{V_{ccmax}}$, where V_{ccmin} is set at a voltage close to V_{knee} of the HBT power stage.

2.3 ET Modulator

As shown in Fig. 8, the ET modulators are categorized into the following three types: i) linear regulator type (Fig. 8 (a)), ii) switching regulator type (Fig. 8 (b)), and iii) hybrid type that combines a linear regulator with a switching one in parallel (Fig. 8 (c)). The linear regulator type, which is based on a low-voltage-drop regulator (LDO) configuration, can deliver a V_{cc} envelope with a small ripple over a relatively wide frequency range [29]. However, the operating efficiency of the regulator is not better than that of the after-mentioned switching regulator type, especially in a low V_{cc} envelope region.

In contrast, the switching regulator type is very efficient over a wide V_{cc} envelope range, while its operating bandwidth is not so wide because of the switching speed limit of CMOS [30], [31].

The hybrid type has advantages of both the linear and switching regulator types and is well suited for handling wide-bandwidth and high-PAPR envelope signals such as 5G NR [32]–[34]. In the hybrid type, the linear regulator works as a voltage source and amplifies the envelope input while maintaining a specified gain and linearity. In contrast, the switching regulator works as a current source and provides most of envelope power at low frequencies for the PA. The sense- and control-block adjusts the output distribution between the linear and the switching regulators. Next, we explain why the hybrid type is suitable for 5G NR using a power spectrum of a CP-OFDM QPSK 100 MHz full resource block modulated signal used in 5G NR.

Figure 9 shows an example of the power spectrum and its corresponding power cumulative distribution function for the envelope signal under a CP-OFDM QPSK 100 MHz full resource block modulated signal. We can see that the bandwidth observed is as wide as approximately 300-500 MHz, and this is 3-5 times wider than the nominal bandwidth of 100 MHz in an RF signal band. At first glance, it seems that this wide bandwidth greatly degrades the efficiency of the switching regulator in the hybrid type. However, a second look confirms that most of the power is concentrated in the frequency range from DC to 100 MHz. Therefore, if the hybrid type has a bandwidth of 100 MHz or more, it is expected to operate with high efficiency for this envelope signal. Here, we should note that it is not easy to keep both wideband and high-efficiency operation in the hybrid type. The reason is as follows. High frequency operation for the switching regulator involves high frequency operation for the linear regulator, which lead to the efficiency degradation of the linear regulator. This is because the linear regulator needs to consume current dissipation so as to keep low

output impedance over the required wideband. Thus, the efficiency of the hybrid type is often limited by the efficiency of the linear regulator.

3. Progress of Envelope Tracking Power Amplifier

This section overviews the recent progress in ETPAs for handset applications. In the last 10 years, ETPAs with the hybrid type ET modulators have been actively studied because of their promising capability of wideband and high efficiency operation. Most of the studies are focused on a simultaneous pursuit of wideband and high efficiency operation. In other words, many studies focused on how to carry out the linear and/or switching regulator design and implementation for the pursuit.

Table 1 compares the recent research on ETPAs. The first ETPA for 4G was published in 2012 [35]. The ET modulator in [35] receives an envelope signal with a reduced bandwidth and then supplies it for the linear regulator, thereby reducing power loss inside the ET modulator. The efficiency of the ET modulator is as high as 82% under a modulated signal condition of 10 MHz LTE.

After that, studies on ETPAs that use both APT and ET modes were focused on, because both the modes become available to the usual handsets [37], [38]. One of the studies reported on a 80-MHz wide bandwidth ET operation acceptable for LTE-advanced. The efficiency of the ET modulator is as high as 81.2% and the ACLR of the ETPA is as low as −38.1 dBc under an 80-MHz LTE-advanced condition. Here, the 80-MHz signal comprises four component carriers, where one component carrier has a 20-MHz bandwidth.

The first 5G NR ETPA was reported in [39]. In [39], the ET modulator consists of two buck-converters and a linear regulator, where the converters and regulator are connected in parallel. The two buck-converters operate with different switching frequencies in order to cover low- and mid-frequency ranges. The linear regulator supports a high-frequency range. Thus, this ET modulator operates with a wide bandwidth of 100 MHz that is necessary for 5G NR while delivering a high efficiency of 77%. With a DPD, the ETPA can deliver good ACLR (E-UTRA) of less than −38 dBc under a 100-MHz 5G NR signal condition. In addition, while addressing output power class-2, this ETPA supports GSM, W-CDMA, and LTE as well as 5G NR, and also covers both APT and ET modes. Therefore, we can say that this ETPA is the first report that is quite useful for practical use in the 5G era.

Table 1 Comparison of recent ETPAs.

	Supprot Modulate signals	Operation Mode	PA Power Class	Maximum bandwidth	Maximum Modulator Efficiency	E-UTRA ACLR
2019 ISSCC Samsung [39]	5G NR, LTE, W-CDMA, GSM	ET, APT	Class2	100 MHz	83%@LTE, 10 MHz, 800mW 77%@5G NR, 100 MHz, 800mW	-39 dBc -38 dBc
2018 ISSCC MTK [38]	LTE, W-CDMA, GSM	ET, APT	Class2	80 MHz	87.1%@LTE, 20 MHz, 3W 81.2%@LTE, 80 MHz, 3W	- -38.1 dBc
2018 ISSCC Samsung [37]	LTE, W-CDMA, GSM	ET, APT	Class2	40 MHz	82%@LTE, 40 MHz, 800mW	-38 dBc
2014 ISSCC STMicro [36]	LTE	ET	-	10 MHz	86%@LTE, 10 MHz, 1.8W	-40 dBc
2012 ISSCC UCSD [35]	LTE	ET	-	10 MHz	82%@LTE, 20 MHz, 1.8W	-41 dBc

4. Challenge for Wideband Envelope Tracking Operation

This section gives a description of hot technical challenges and their countermeasure example in handset ETPAs. In the previous Sects. 2 and 3, the recent approaches toward realizing wideband operation in the ET modulators are given in details. Regarding the wideband operation of the PAs, one of the hottest technical challenges is a memory effect. Another technical challenge is how to use APT and ET modes for the ETPA under a 100-MHz 5G NR modulated signal condition. In regard to these two challenges, we introduce our countermeasure example while demonstrating the latest measurements for an in-house ETPA prototype.

4.1 Memory Effect

In general, nonlinear devices such as transistors having non-flat frequency response have an electrical memory effect. The signal distortion due to this memory effect becomes larger as the modulated signal bandwidth is wider, like 100-MHz 5G NR. In addition, in transistors having a thermal time constant, a thermal memory effect is observed. In particular, it is well known that transistors having many deep traps show complicate thermal memory effects. The thermal memory effect depends on device junction temperature history, influencing transient response in the PAs.

In handset PAs with GaAs-based HBTs, we often experience the signal distortion due to the electrical memory effect rather than the distortion due to the thermal memory effect. This is because the HBT is a bulk conductive device, not a surface conductive one, and has a relatively fast thermal time constant. We, therefore, have concentrated on low-impedance design for the bias circuit at low frequencies in order to suppress signal distortions, e.g. intermodulation distortions (IMD) such as IMD3 and IMD5 during the PA design [40].

Figures 10 (a) and (b) show output spectra for handset HBT PAs measured using 5G NR 2.6-GHz-band DFTs (Discrete Fourier Transform spreading)-OFDM QPSK signals having bandwidths of 20 MHz and 100 MHz, respectively. The measurement was performed at a V_{cc} of 5.0 V. The figures clearly indicate that the distortion levels for the

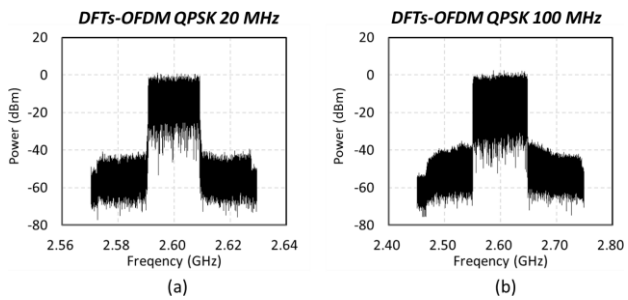

Fig. 10 Output spectra of the PA: (a) 20 MHz and (b) 100 MHz.

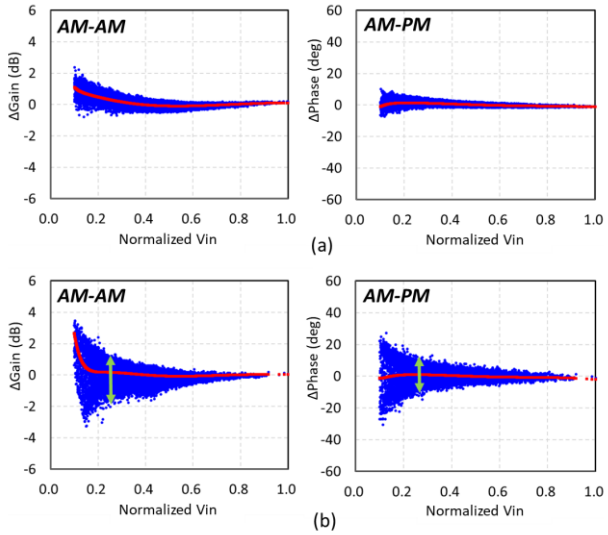

Fig. 11 Dynamic AM-AM and AM-PM characteristics of the PA: (a) 20 MHz, and (b) 100 MHz.

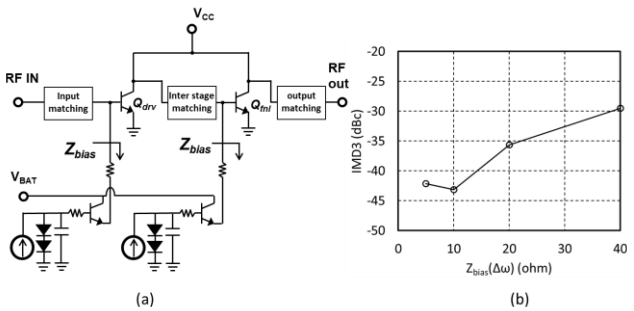

Fig. 12 Simulated third-order intermodulation distortion: (a) simplified schematic and (b) IMD3 versus the bias network impedance.

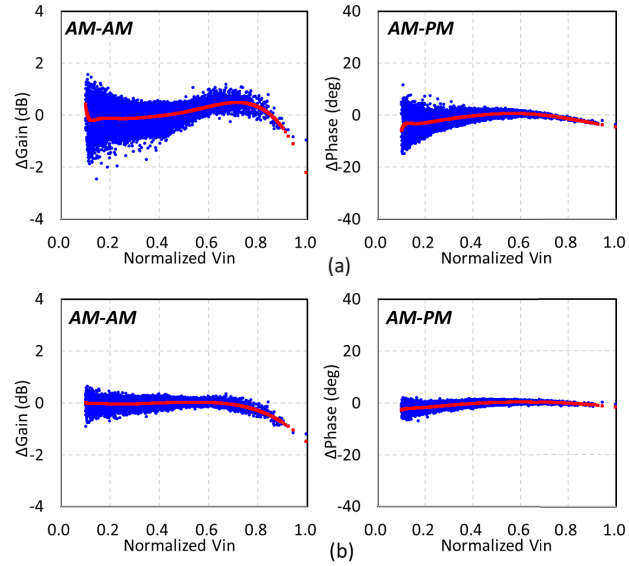

Fig. 13 Dynamic AM-AM and AM-PM characteristics of the PA under DFTs-OFDM QPSK 100 MHz modulated signal: (a) before and (b) after optimization for the bias network impedance.

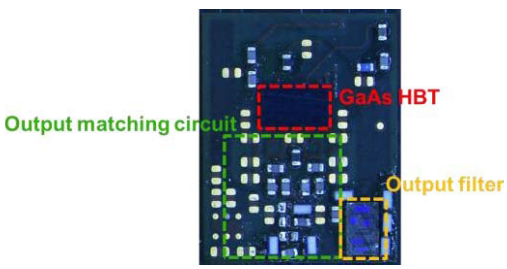

Fig. 14 Micrograph of the prototype PA module with output filter.

100-MHz wideband are larger than those for the 20-MHz narrowband signal.

Figure 11 shows dynamic AM-AM and AM-PM characteristics under the same measurement condition as in Fig. 10. As indicated in the green arrows, the dispersion of the signal distortion for the 100-MHz signal is quite larger than that for the 20-MHz signal. We often call this dispersion "Cloud." Such a large Cloud often prevents a memory-less DPD from compensating for the AM-AM/AM-PM characteristics in the PAs. It is, therefore, very important to suppress such a Cloud sufficiently in a PA design step.

Low-impedance design for the bias circuit at low frequencies is effective in suppressing IMD. Next, our low-impedance design and its related measurements are described as a countermeasure for wideband modulated signals such as 5G NR.

Figure 12 (a) shows the simplified schematic for the HBT PA, and Fig. 12 (b) shows IMD3 versus simulated impedance seen from the HBT power stage toward the bias circuit. The IMD3 simulation was carried out using a 2.6-GHz-band two-tone signal with an offset frequency of 100 MHz. Figure 12 (b) clearly indicates that low impedance design of the bias circuit is very effective for IMD3 suppression.

Measured dynamic AM-AM/AM-PM characteristics for two HBT PAs fabricated in this study are compared in Fig. 13, where one PA is the same as used in Fig. 10 and low impedance design was not applied. In contrast, to the other PA, low impedance design shown in Fig. 12 (b) was applied. The HBT PA with low impedance shows smaller Cloud than the HBT PA without low impedance does under the condition of a DFTs-OFDM QPSK 100-MHz modulated signal, V_{cc} = 5V, and P_{out} = 30dBm. In addition to the simulation, the measurement proves that the low-impedance design for the bias circuit is one of the most effective ways to suppress the Cloud for wideband modulation signals.

Next, we demonstrate the latest measurements for our new prototype 5G NR ETPA operating in a 2.6-GHz band. The micrograph for the PA module block fabricated on a FR-4 laminate is shown in Fig. 14. The PA module block consists of a two-stage GaAs-HBT MMIC, several SMDs, and an output band-pass filter. As shown in the micrograph, the output matching circuit block is followed by the filter used for practical 5G TDD operation. Taking into account a front-end loss of 2 dB between the filter and an antenna, the

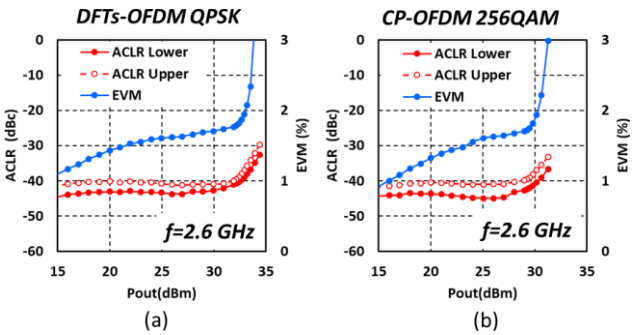

Fig. 15 Measured ACLR and EVM characteristics: (a) DFTs-OFDM QPSK, and (b) CP-OFDM 256QAM.

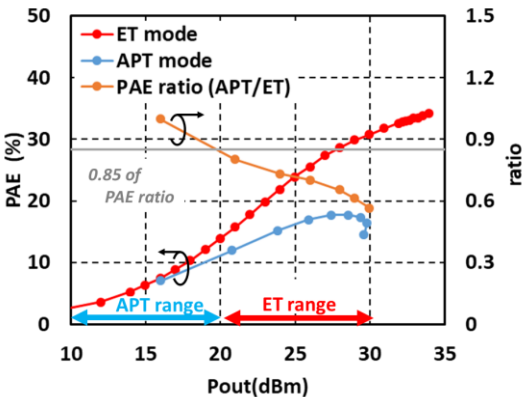

Fig. 16 Efficiency comparison between ET mode and APT mode.

target output power was set at 32 dBm. This target can meet HPUE (High Power User Equipment) Power Class-2 (PC2) specifications under the condition of DFTs-OFDM QPSK 100 MHz full resource blocks and MPR (Maximum Power Reduction) = 1. HPUE PC2 is a new LTE power standard with 3GPP specifications to improve LTE TDD transmission area.

A National Instrument PXI signal generator/analyzer series was used for the measurements. Figure 15 shows the measured ACLR and EVM versus output power characteristics for the ETPA. The modulated signals used here are a DFTs-OFDM QPSK 100 MHz signal (MPR = 1) and a CP-OFDM 256QAM 100 MHz signal (MPR = 6.5). The DPD was used in the memoryless DPD mode for emulating practical distortion compensation. As shown in Fig. 15, the ETPA can deliver an output power of 32 dBm and ACLR of less than −40 dBc for a DFTs-OFDM QPSK 100 MHz modulated signal (MPR = 1). The ETPA can also deliver an EVM as good as 1.7% for a CP-OFDM 256QAM 100 MHz signal (MPR = 6.5). Thus, the prototype ETPA satisfies strict specifications required for 5G NR handset PAs.

4.2 Efficiency Performance for APT vs ET

As mentioned previously, both APT and ET modes are used in practical handset use. This subsection describes how to determine output power ranges of the APT and ET modes.

Measured efficiency for the ETPA shown in Fig. 14 was shown in Fig. 16, where efficiencies in the APT and ET modes that satisfy ACLR of less than −40 dBc are plotted under the DFTs-OFDM QPSK 100 MHz modulated signal condition. The efficiency ratio of APT to ET is also plotted. In the APT mode, the supply voltage step is 0.5 V and the voltage sweep ranges from 1.0 V to 5.0 V.

As shown in the figure, in the high power range, the PA in the ET mode can deliver more than 10 percentage points higher than the PA in the APT mode can. In addition, the PA in the ET mode is able to deliver higher output power than the PA in the APT mode.

The latest paper reports on an efficiency of 77% for the ET modulator [39], whereas the usual DC-DC converter used in the APT mode exhibits an average efficiency of 95% under a high output current condition. Considering these two efficiency plots, in the power range where the efficiency ratio is more than 0.85, the ETPA operates with higher overall efficiency than the PA in the APT mode does. On the other hand, in the power range of the ratio of less than 0.85, the PA in the APT mode becomes more efficient than the ETPA.

Thus, we can determine the optimum power range for the APT and ET modes.

5. Conclusion

This paper describes the recent progress in ET power amplifiers (ETPAs) while giving the introduction of a basic operation for an ET modulator as well as some kinds of ET modulators. In addition, this paper also demonstrates the latest experimental results for a 5G ETPA prototype while comparing overall efficiency between the ET and APT modes.

We expect that the ET techniques presented here will contribute to the realization of smaller-size and high efficient ETPAs for 5G and beyond 5G handset applications.

Acknowledgements

The author would like to thank Y. Noguchi, K. Takenaka, H. Matsumoto, J. Enomoto, Y. Tanaka, F. Harima, and S. Arayashiki of Murata Manufacturing Co., Ltd., for their fruitful discussions.

References

[1] 3GPP TS 38.101-1 V15.6.0, 3rd Generation Partnership Project; Technical Specification Group Radio Access Network; NR; User Equipment (UE) radio transmission and reception; Part 1: Range 1 Standalone, June 2019.
[2] F. Balteanu, H. Modi, Y. Choi, J. Lee, S. Drogi, and S. Khesbak, "5G RF front end module architectures for mobile applications," IEEE EuMC., pp.252–255, Oct. 2019.
[3] K. Yamamoto, T. Moriwaki, H. Otsuka, N. Ogawa, K. Maemura, and T. Shimura, "A CDMA InGaP/GaAs-HBT MMIC power amplifier module operating with a low reference voltage of 2.4V," IEEE J. Solid-State Circuits, vol.42, no.6, pp.1282–1290, June 2007.
[4] D. Kang, D. Yu, K. Min, K. Han, J. Choi, D. Kim, B. Jin, M. Jun, and B. Kim, "A highly efficient and linear Class-AB/F power amplifier for multimode operation," IEEE Trans. Microw. Theory Techn.,

vol.56, no.1, pp.77–87, Jan. 2008.
[5] G. Hau, S. Hsu, Y. Aoki, T. Wakabayashi, N. Furuhata, and Y. Mikado, "A 3x3mm^2 embedded-wafer-level packaged WCDMA GaAs HBT power amplifier module with integrated Si DC power manegement IC," IEEE RFIC, pp.409–412, April 2008.
[6] K. Mukai, S. Shinjo, K. Yamanaka, M. Miyashita, and K. Yamamoto, "A Dual-Gain-Mode high efficiency power amplifier for W-CDMA data communication," IEEE APMC, pp.671–673, Nov. 2014.
[7] J.P Young and N. Cheng, "Multimode mutiband power amplifier optimization for mobile applications," VLS-TSA, pp.1–3, April 2013.
[8] T. Gillenwater and M. Schindler, "Technology trends in mobile handsets," IEEE IWS, pp.1–4, April 2013.
[9] J. Jeon, J. Oh, J. Jung, and S. Paek, "Multimode multiband power amplifier module integrated duplexer for mobile applications," IEEE RFIT, pp.110–112, Aug. 2017.
[10] K. Yamamoto, T. Matsuzuka, M. Miyashita, K. Maeda, S. Suzuki, and H. Seki, "0.8-/1.5-GHz-Band WCDMA HBT MMIC power amplifier with an analog bias control scheme," IEICE Trans. Electron., vol.98-C, no.9, pp.934–945, Sept. 2015.
[11] A.A.M. Saleh and D.C. Cox, "Improving the power-added efficiency of FET amplifiers operating with varying envelope signals," IEEE Trans. Microw. Theory Techn., vol.31, no.1, pp.51–55, Jan. 1983.
[12] B.D. Geller, F.T. Assal, R.K. Gupta, and P.K. Cline, "A technique for the maintenance of FET power amplifier efficiency under back-off," IEEE MTT-S Int. Microwave Symp. Digest., pp.949–952, June 1989.
[13] G. Hanington, P.-F. Chen, P.M. Asbeck, and L.E. Larson, "High-efficiency power amplifier using dynamic power-supply voltage for CDMA applications," IEEE Trans. Microw. Theory Techn., vol.47, no.8, pp.1471–1476, Aug. 1999.
[14] J.H. Qureshi, W. Sneijers, R. Keenan, L.C.N. de Vreede, and F. van Rijs, "A 700-W peak ultra-wideband broadcast doherty amplifier," IEEE MTT-S Int. Microwave Symp., pp.1–4. June 2014.
[15] F. Wang, A. Ojo, D. Kimball, P.M. Asbeck, and L. Larson, "Envelope tracking power amplifier with pre-distortion for WLAN 802.11g," IEEE MTT-S Int. Microwave Symp. Digest., pp.1543–1546, June 2004.
[16] C.D. Presti, A.G. Metzger, H.M. Banbrook, P.J. Zampardi, and P.M. Asbeck, "Efficiency improvement of a handset WCDMA PA module using adaptive digital predistortion," IEEE MTT-S, pp.804–807, June 2010.
[17] R.N. Braithwaite, "Closed-loop digital predistortion (DPD) using an observation path with limited bandwidth," IEEE Trans. Microw. Theory Techn., vol.63, no.2, pp.726–736, Feb. 2015.
[18] P.J. Draxler, J. Deng, D. Kimball, I. Langmore, and P.M. Asbeck, "Memory effect evaluation and predistortion of power amplifiers," IEEE MTT-S, pp.1549–1552, June 2005.
[19] P.J. Draxler, A. Zhu, J.J. Yan, P. Kolinko, D.F. Kimball, and P.M. Asbeck, "Quantifying distortion of RF power amplifiers for estimation of predistorter Performance," IEEE MTT-S., pp.931–934, June 2008.
[20] S. Tanaka, "A new decomposition method of LC-ladder matching circuits with negative components," IEICE Trans. Fundamentals, vol.E103-A, no.9, pp.1011–1017, Sept. 2020.
[21] G.T. Watkins and K. Mimis, "Impact of envelope shaping on the linearitiy of envelope tracking transmitters," IET Annual Active and Passive RF Devices Seminar., Oct. 2014.
[22] J. Choi, D. Kim, D. Kang, and B. Kim, "A polar transmitter with CMOS programmable hysteretic-controlled hybrid switching supply modulator for multistandard applications," IEEE Trans. Microw. Theory Techn., vol.57, no.7, pp.1675–1686, July 2009.
[23] J. Kim, J. Son, S. Jee, S. Kim, and B. Kim, "Optimisation of envelope tracking power amplifier for base-station applications," IEEE Trans. Microw. Theory Techn., vol.61, no.4, pp.1620–1627, July 2011.
[24] D. Kim, D. Kang, J. Choi, J. Kim, Y. Cho, and B. Kim, "Optimization for envelope shaped operation of envelope tracking power amplifier," IEEE Trans. Microw. Theory Techn., vol.59, no.7, pp.1787–1794, July 2011.
[25] Y. Lin, H. Jang, C. Quindroit, N. Naraharisetti, and P. Roblin, "New supply modulation optimization methodology for concurrent dual band envelope tracking power amplifier," IEEE WAMICON., pp.1–4, June 2014.
[26] J.-L. Woo, S. Park, and Y. Kwon, "A wideband envelope-tracking CMOS linear transmitter without digital predistortion," IEEE RFIC., pp.367–370, June 2015.
[27] J. Jeong, D. Kimball, M. Kwak, C. Hsia, P. Draxler, and P. Asbeck, "Modeling and design of RF power amplifiers for envelope tracking WCDMA base-station Applications," IEEE Trans. Microw. Theory Techn., vol.57, no.9, pp.2148–2159, Sept. 2009.
[28] D. Kimball, J. Jeong, C. Hsia, P. Draxler, S. Lanfranco, W. Nagy, K. Linthicum, L. Larson, and P. Asbeck, "High-efficiency envelope tracking W-CDMA base-station amplifier using GaN HFETs," IEEE Trans. Microw. Theory Techn., vol.54, no.11, pp.3848–3856, Nov. 2006.
[29] P. Reynaert and M.S.J. Steyaert, "A 1.75GHz polar modulated CMOS RF power amplifier for GSM-EDGE," IEEE J. Solid-State Circuits, vol.40, no.12, pp.2598–2608, Dec. 2005.
[30] R. Shrestha, R.A.R. Van der Zee, A.J.M. Graauw, and B. Nauta, "A wideband supply modulator for 20MHz RF bandwidth polar Pas in 65nm CMOS," IEEE J. Solid-State Circuits, vol.44, no.4, pp.1272–1280, April 2009.
[31] F. Wang, D.F. Kimball, D.Y. Lie, P.M. Asbeck, and L.E. Larson, "A monolithic high-efficiency 2.4-GHz 20-dBm SiGe BiCMOS envelope-tracking OFDM power amplifier," IEEE J. Solid-State Circuits, vol.42, no.6, pp.1271–1281, June 2007.
[32] Y. Li, J. Lopez, D.Y.C. Lie, K. Chen, S. Wu, T.-Y. Yang, and G.-K. Ma, "Circuits and system design of RF polar transmitters using envelope-tracking and SiGe power amplifiers for mobile WiMAX," IEEE Trans. Circuits Syst. I, Reg. Papers, vol.58, no.5, pp.893–901, May 2011.
[33] G.B. Yundt, "Series- or parallel-connected composite amplifiers," IEEE Trans. Power Electron., vol.PE-1, no.1, pp.48–54, Jan. 1986.
[34] J. Choi, D. Kim, D. Kang, and B. Kim, "A new power management IC architecture for envelope tracking power amplifier," IEEE Trans. Microw. Theory Techn., vol.59, no.7, pp.1796–1802, July 2011.
[35] M. Hassan, L. Larson, V. Leung, and P. Asbeck, "A combined series-parallel hybrid envelope amplifier for enveloope tracking mobile terminal RF power amplifier applications," IEEE J. Solid-State Circuits, vol.47, no.5, pp.1185–1198, May 2012.
[36] P. Amò, M. Thomas, V. Molata, and T. Jeřábek, "Envelope modulator for multimode transmitters with AC-coupled multilevel regulators," IEEE ISSCC, pp.296–297, Feb. 2014.
[37] T. Nomiyama, Y. Youn, Y. Choo, D. Kim, J. Han, J. Jung, J. Baek, S. Lee, E. Park, J. Choi, J. Paek, J. Lee, T. Cho, and I. Kang, "A 2Tx supply modulator for envelope-tracking power amplifier supporting intra- and inter-band uplink carrier aggregation and power class-2 high-power user equipment," IEEE ISSCC, pp.434–435, Feb. 2018.
[38] C.-Y. Ho, S.-M. Lin, C.-H. Meng, H.-P. Hong, S.-H. Yan, T.-H. Kuo, C.-S. Peng, C.-H. Hsiao, J.-H. Chen, D.-W. Sung, and C.-W. Kuan, "An 87.1% efficiency RF-PA envelope-tracking modulator for 80MHz LTE-advanced transimtter and 31dBm PA output power for HPUE in 0.153μm CMOS," IEEE ISSCC, pp.432–433, Feb. 2018.
[39] J. Paek, D. Kim, J. Bang, J. Baek, J. Choi, T. Nomiyama, J. Han, Y. Choo, Y. Youn, E. Park, S. Lee, I. Kim, J. Lee, T. Cho, and I. Kang, "An 88%-efficiency suply modulator achieving 1.08μs/V fast transition and 100MHz envelope tracking bandwidth for 5G new Radio RF power amplifier," IEEE ISSCC, pp.238–239, Feb. 2019.
[40] J. Deng, P. Gudem, L. Larson, D. Kimball, and P. Asbeck, "A SiGe PA with dual dynamic bias control and memoryless digital predistortion for WCDMA handset applications," IEEE J. Solid-State Circuits, vol.41, no.5, pp.1210–1221, May 2006.

Kenji Mukai received the B.S. degree in physics from Osaka City University, Osaka, Japan in 2004, and the M.S. degree in physics from Osaka University, Toyonaka, Japan in 2006. In 2006, he joined Mitsubishi Electric Corporation, Itami, Japan, where he had been engaged in the research and development of GaAs HBT and GaN HEMT power amplifier for mobile communication. Between 2012 and 2013, he was a Visiting Scholar at the University of California, San Diego where he researched GaN HEMT switching mode power amplifier for envelope tracking and digital transmitter. In 2017, he moved to the RF Device Division, Murata Manufacturing Co., Ltd. and he is developing PAMiD and PAMiF for 5G NR. His current research interests are GaAs- and Si-based RF MMIC front-ends module and their efficiency enhancement technique. He is a member of the IEICE and a member of the IEEE.

Hiroshi Okabe received the B.S. and M.S. degrees from The University of Electro-Communications, Tokyo, Japan, in 1990 and 1992, respectively. From 1992 to 2012, he was with Central Research Laboratory, Hitachi, Ltd., Tokyo, Japan, where he was engaged in the research and development of cellular handsets, built-in antennas, and RF front-end modules. From 2001 to 2002, he was a Visiting Scholar in the Electrical Engineering Department at the University of California, Los Angeles, where he researched circuit applications of metamaterials. In 2012, he joined Murata Manufacturing Co., Ltd., Kyoto, Japan. Currently, he is leading the research and development of power amplifier ICs and front-end solutions for the latest cellular handsets. Mr. Okabe is a member of the IEICE, and a member of the IEEE.

Satoshi Tanaka has received BS and MS degree in 1983 and 1985, from Waseda University, and Ph.D. (Engineering) degree in 2019 from Tohoku University respectively. In 1985, he joined Central Research Laboratory, Hitachi, Ltd. He was engaged in research and development on mixed analog and digital bipolar CMOS, GaAs ICs, CMOS and Bi-CMOS RFICs for GSM and W-CDMA applications. In 2006, he moved to Renesas Technology Corp. and developed power amplifier for mobile phone with LDMOS and HBT. From 2012, he has joined Murata Manufacturing Co., Ltd. Currently he is developing RF front-end modules especially multi-band multi-mode PA modules for GSM/W-CDMA/LTE/5G. During 2005–2009, he had been the technical committee member of IEEE ISSCC. During 2009–2018, he has been a RF program committee chair of IEEE A-SSCC. In 2015 he was a chair of Technical Committee on Circuits and Systems (CAS), IEICE. He is a senior member of the IEICE and of the IEEE.